Met. Mater. Int., Vol. 20, No. 6 (2014), pp. 1011~1016
doi: 10.1007/s12540-014-6003-9

Effects of Milling Media on the Mechanical Properties of Gas Pressure Sintered α/β-SiAlON

Sungsu Chun[1], Bong-Ki Min[2], and Sukyoung Kim[1,*]

[1]Yeungnam University, School of Materials Science and Engineering, Gyeongsan 712-749, Korea
[2]Yeungnam University, Center for Research Facility, Gyeongsan 712-749, Korea

(received date: 24 December 2013 / accepted date: 10 February 2014)

Three types of milling media, alumina, zirconia and cemented tungsten carbide (CTC), were used for the solid-state preparation of SiAlON from Si_3N_4 using Y_2O_3-Al_2O_3-AlN as sintering aids. Fully densified α and β dual-phase SiAlON composites were obtained by gas pressure sintering (GPS) at 1750 °C for 1.5 hrs. The relative contents of α- and β-SiAlON and grain boundary phases in the sintered samples were affected by the type of milling media, where the main grain boundary phases were α-, β-SiAlON and melilite ($Y_2Si_3O_3N_4$). Zirconium nitride was observed at the grain boundaries of the samples prepared using zirconia media, and WC and Co_3W_3C were observed with the sample prepared using CTC media due to contamination from the milling media. As a result, the overall mechanical properties, color, and microstructure of SiAlON were affected by the grain boundary phases and the α- to β-SiAlON ratio. The SNZ sample prepared using ZrO_2 media showed better mechanical properties than the SNA and SNW samples. These results were compared with those obtained by spark plasma sintering, which was reported previously.

Keywords: ceramics, mechanical alloying/milling, optical properties, scanning/transmission electron microscopy (STEM), hardness test

1. INTRODUCTION

SiAlON is a high temperature ceramic that is a form of solid-solution between Si_3N_4 and Al_2O_3, where Si and N in Si_3N_4 are replaced with Al and O, respectively. The crystal structure of α- and β-SiAlON is the same as that of α- and β-Si_3N_4, respectively. The sintering of this material is generally performed through transient liquid-phase sintering after adding Y (yttrium) because α-SiAlON can incorporate rare-earth elements [1]. The wear-resistance of Y-added α- and β-SiAlON was reported to be different. α-SiAlON is suitable for use under mild wear conditions, whereas under more severe conditions, β-SiAlON shows better wear-resistance than α-SiAlON [2]. Therefore, if the composites are composed of both α- and β-SiAlONs, the composite (α/β-SiAlON) can be used in a wider range of applications with better wear-resistance properties over single phase α- or β-SiAlON. Therefore, α/β-SiAlON composites have become an important material for many applications, such as metal cutting, wire drawing, extrusion, thermal protection and high temperature wear parts applications, particularly at high temperatures (600-1400 °C). The high temperature mechanical properties, such as hardness, fracture toughness and strength, are very important for ensuring the reliability for high temperature applications

Considerable efforts have been made to α/β-SiAlON synthesis for cutting tool applications owing to its superior hardness compared to silicon nitride ceramics. For example, the inclusion of hard particles, such as SiC was evaluated to improve the wear resistance and life time of α/β-SiAlON further [3]. In addition, various rare-earth oxides (Y_2O_3, Sm_2O_3, La_2O_3, Yb_2O_3, and Er_2O_3) have been tested to enhance the sinterability of SiAlON. The Y_2O_3-Al_2O_3-AlN system was found to be the most successful sintering aid so far [4,5]. The effects of the grain boundary phases have also been investigated because the association of these grain boundary phases with these sintering aids can affect the mechanical and optical properties of SiAlON [4-7]. In addition to the effects of sintering aids, other factors that can also affect the grain boundary phases include contamination from the milling media during the milling process. The milling process is an inevitable process in the industrial production of SiAlON via a solid-state reaction.

Previous studies reported the effects of various milling media on the hardness, phase contents and physical properties of α/β-SiAlON consolidated by a spark plasma sintering (SPS) [8]. As part of a continuing study, this study examined

*Corresponding author: sykim@yu.ac.kr

the effects of three types of milling media on the mechanical properties of α/β-SiAlON sintered by a gas pressure sintering method (GPS). The GPS technique is more desirable for industrial mass production than SPS. The mechanical properties of α/β-SiAlON, such as high temperature hardness, fracture toughness, elastic modulus, Poisson's ratio, flexural strength, and Weibull modulus, were evaluated. The results obtained by GPS were compared with the results by SPS.

2. EXPERIMENTAL PROCEDURE

Si_3N_4 (UBE, Grade SN-E10), AlN (H. C. Starck, Grade C), Al_2O_3 (Sumitomo, Grade AKP-30) and Y_2O_3 (H. C. Starck, Grade C) were used as the starting materials for the fabrication of the α/β-SiAlON composites. After weighing to a stoichiometric SiAlON composition containing 15 wt% of Y_2O_3-Al_2O_3-AlN sintering aids, 4 wt% of PVA binder was added. Three batches of the powder mixture were ball-milled for 24 h in ethanol using 8 mm Al_2O_3, 8 mm ZrO_2 and 6 mm CTC milling media. The Al_2O_3, ZrO_2 and CTC balls contained SiO_2, Y_2O_3 and Co as a sintering aid, respectively. The detailed specifications and microstructures for three kinds of milling media can be found in our previous report [8]. The ball-milled slurries were dried at 50 °C in a rotary spray dryer and then pressed into rectangular blocks or pellets using a uniaxial press at 120 MPa. Sintering was performed by gas pressure sintering (KOBELCO, PSF-350, Japan) for 1.5 h at 1750 °C under a N_2 gas pressure of 50 bar. The SiAlON samples prepared using alumina, zirconia and cemented tungsten carbide (CTC, WC containing 10 wt% Co) as milling media are hereinafter called SNA, SNZ and SNW, respectively.

The sintered density of the specimens was measured according to the Archimedes' principle. The color properties of the polished samples were determined using a UV-visible spectrophotometer (Minolta 3700d) according to the colorimetric method recommended by CIE (Commission Internationale d'Eclairage) [8,12]. The phases existing in the composites were confirmed by a X-ray diffraction (XRD, MPD, PANalytical) and the relative amount of α- and β-SiAlON phases was calculated by a quantitative estimation from the integrated intensities of the (102) and (210) reflections for α-SiAlON and β-SiAlON, as described elsewhere [9]. The microstructures of the samples were observed by scanning electron microscopy (SEM; 7600F, JEOL) and transmission electron microscopy (TEM; Tecnai F20, FEI). The specimens for TEM analysis were prepared using a dual-beam focused ion beam (FIB; Quanta 3D, FEI). A back-scattered electron detector (BSE) in SEM was used because it can easily confirm the different elements in the grains. High-angle annular dark-field imaging (HAADF) scanning transmission electron microscopy (STEM), which is highly sensitive to variations in the atomic number of atoms in the sample, was used for elemental analysis of the grains. TEM bright-field (BF) and dark-field (DF) observations were used and the crystal structures were analyzed from the DF observations. The Vickers hardness was measured under a 98 N load (DVK, Matsuzawa, Japan). The fracture toughness was also determined using the indentation fracture method with an applied load of 98 N, according to the equation reported by Lawn and Fuller [10]. The four-point bending strength and Weibull modulus were estimated in accordance with ASTM C1161 and ASTM C1239 for 50 pieces of rectangular bars (3.0 mm×4.0 mm×45.0 mm). The Young's modulus and Poisson's ratio were measured by resonant ultrasound spectroscopy (Modulus 2, Dynamic Resonance System Co. USA) using a rectangular specimen (5.0 mm×4.8 mm×4.5 mm) after grinding the samples with #2,000 diamond grit. The hot hardness was also measured three times using a 1 kg_f load (AVK-HP, Akashi, Japan) at 300, 600 and 900 °C in a N_2 atmosphere for the square-blocked sample (10.0 mm×10.0 mm ×4.0 mm).

3. RESULTS AND DISCUSSION

The weight gain of the powder during the milling was 0.16, 0.96 and 1.16% for the SNA, SNZ and SNW samples, respectively. A noticeable color difference of the samples was observed depending on the milling media used due to contamination, which is similar to the samples consolidated by SPS [8]. Table 1 lists the color properties of the three samples, where L^* indicates the lightness of the color ranging from white (L^*=100) to black (L^*=0). The chromaticity a^* represents the color from green ($-a^*$) to red ($+a^*$), and b^* indicates the color from blue ($-b^*$) to yellow ($+b^*$). The lightness (L^*) decreased in the order of SNA (46.17), SNZ (42.37) and SNW (41.97) for the GPS-sintered samples, which is the same trend as the samples sintered by SPS [8]. The difference in color was attributed to different inclusions and grain boundary phases, which originated from the wear debris of the milling media. The SNA samples prepared by GPS were darker than those by SPS, while the opposite was true for the SNZ and SNW samples. According to Table 1, the samples sintered by GPS showed a slightly different color from those sintered by SPS, in which the polar coordinates are presented in Fig. 1 along with a digital image of the sintered samples prepared by GPS.

The formation of α/β-SiAlON as a main phase of the composites was confirmed by XRD, as shown in Fig. 2. The XRD pattern showed that the composites consisted of α-, β-SiAlON

Table 1. Comparison of the colorimetric analysis results for the samples sintered by GPS and SPS [8]

Specimens	Gas Pressure Sintering (GPS)			Spark Plasma Sintering (SPS)		
	L^* (D65)	a^* (D65)	b^* (D65)	L^* (D65)	a^* (D65)	b^* (D65)
SNA	46.17	–0.76	–0.47	47.82	–0.38	4.5
SNZ	42.37	0.53	1.75	40.55	0.41	1.51
SNW	41.97	0.04	–0.71	39.07	0.00	–0.71

and crystallized grain boundary phases, such as $Y_2Si_3O_3N_4$ and $Y_{10}Al_2Si_3O_{18}N_4$. In addition, the presence of ZrN in the SNZ sample, and WC and Co_3W_3C in the SNW sample was observed, where these phases were formed by a reaction between the debris of the milling media and starting materials, which is similar to the previous results using SPS [8]. Both the SNA and SNZ samples prepared by SPS revealed the presence of α-Si_3N_4 [8], whereas α-Si_3N_4 was not observed with the GPS-sintered samples. This indicates that a complete transformation of Si_3N_4 to SiAlON occurred during GPS sintering because of the adequate holding time of 1.5 h at 1750 °C for GPS compared to 5 min at 1510 °C with SPS. Based on the calculations from XRD, the content of α-SiAlON in the SNA, SNZ and SNW specimens was 27, 19 and 15 wt%, respectively. α, β-SiAlON and melilite ($Y_2Si_3O_3N_4$) phases were observed in the SNA samples, whereas additional secondary phases were detected in the SNZ and SNW samples, such as ZrN, WC, Co_3W_3C and yttrium-rich aluminosilicate ($Y_{10}Al_2Si_3O_{18}N_4$). The amount of liquid phase would be larger in SNA than in SNZ and SNW because alumina was ground into raw materials during milling and reacted with the sintering additives. Although the $Y_{10}Al_2Si_3O_{18}N_4$ phase could not be found with SNA, it is expected that the $Y_{10}Al_2Si_3O_{18}N_4$ phase was formed initially at the grain boundary and then transformed to melilite for this sample. For the SNZ and SNW samples, although the raw materials could be contaminated by zirconia and tungsten carbide including cobalt during milling, this would be different from Al_2O_3 contamination in SNA because ZrO_2, WC and Co rarely form a solid-solution with SiAlON or Si_3N_4 at the grain boundaries.

Figure 3 shows back-scattered SEM images of the polished surface of SNA, SNZ and SNW, where the white, gray and dark gray areas correspond to the grain boundary phase, α-SiAlON and β-SiAlON, respectively. The well-grown β-SiAlON grains were distributed homogeneously in the matrix for

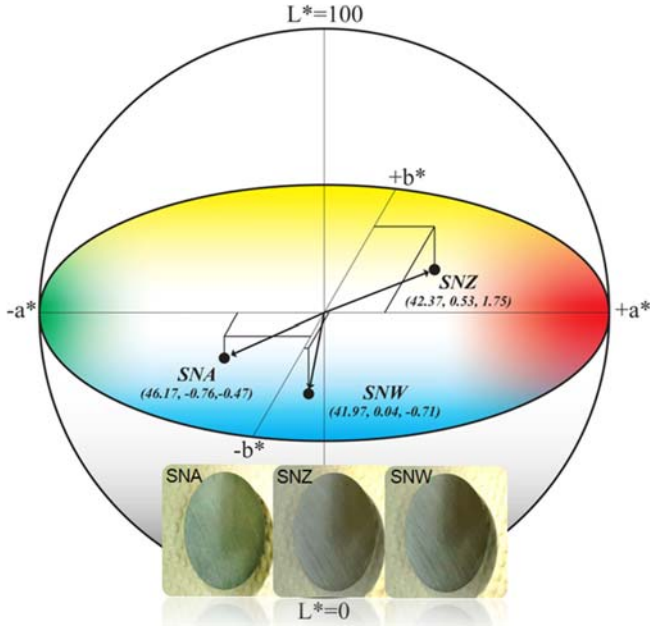

Fig. 1. Polar coordinates representing the L*, a* and b* values for the GPS-sintered SNA, SNZ and SNW along with digital images of the samples.

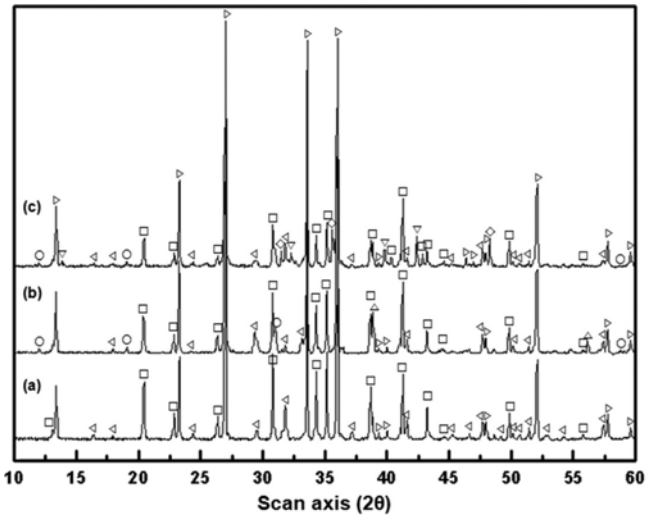

Fig. 2. XRD patterns of sintered α/β-SiAlON for (a) SNA, (b) SNZ and (c) SNW samples. (□) α- SiAlON, (▷) β- SiAlON, (◁) $Y_2Si_3O_3N_4$, (○) $Y_{10}Al_2Si_3O_{18}N_4$, (△) ZrN, (▽) Co_3W_3C, (◇) WC.

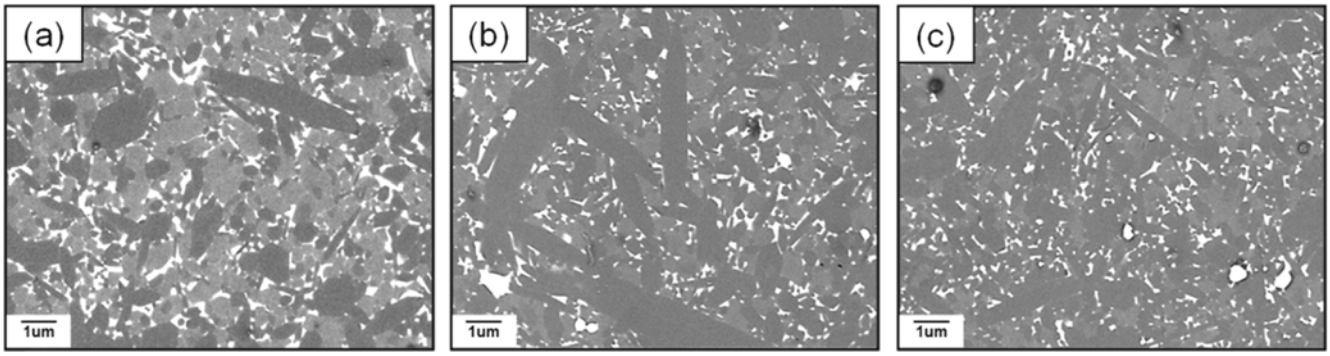

Fig. 3. Back-scattered SEM images of the polished surface for (a) SNA, (b) SNZ and (c) SNW samples, the white, gray and dark gray areas correspond to the grain boundary phase, α-SiAlON and β-SiAlON (magnification X 10,000).

all samples. The ratio of three phases was different, depending upon the samples. The larger amounts of α-SiAlON and grain boundary phases were found in SNA because of the more presence of liquid phase during sintering than the other samples. The SNA and SNZ samples showed the elongated β-SiAlON grains, while the SNW had less elongated and smaller grain size. From our previous report [8], it is believed that the WC ball wear debris promoted the phase conversion from α-Si_3N_4 to β-SiAlON and melilite phases at the grain boundary. The more β-SiAlON phase was formed in the SNW than others. It means that the more β phase seeds were existed in the matrix and consequently hindered the grain growth. Inversely the SNA and SNZ showed elongated β-SiAlON grains than SNW. However, the SNA had smaller elongated β-SiAlON grains because the α-SiAlON phase in the SNA was more formed than that in the SNZ and then hindered the elongated β-SiAlON phase formation and growth.

Figure 4 presents TEM images showing the presence of inclusions formed from the milling media and starting materials in the SNZ and SNW samples. ZrN was formed from

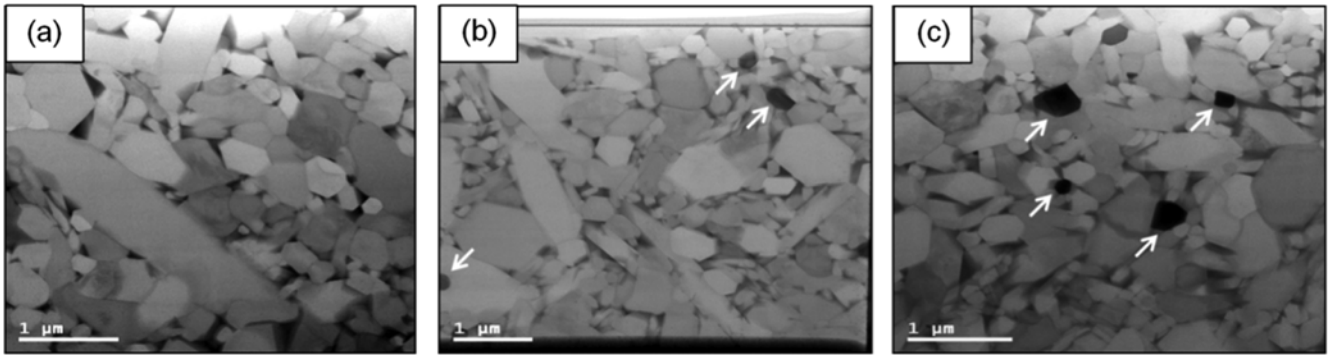

Fig. 4. Bright-field TEM images for (a) SNA, (b) SNZ and (c) SNW samples (wear debris are marked using arrows).

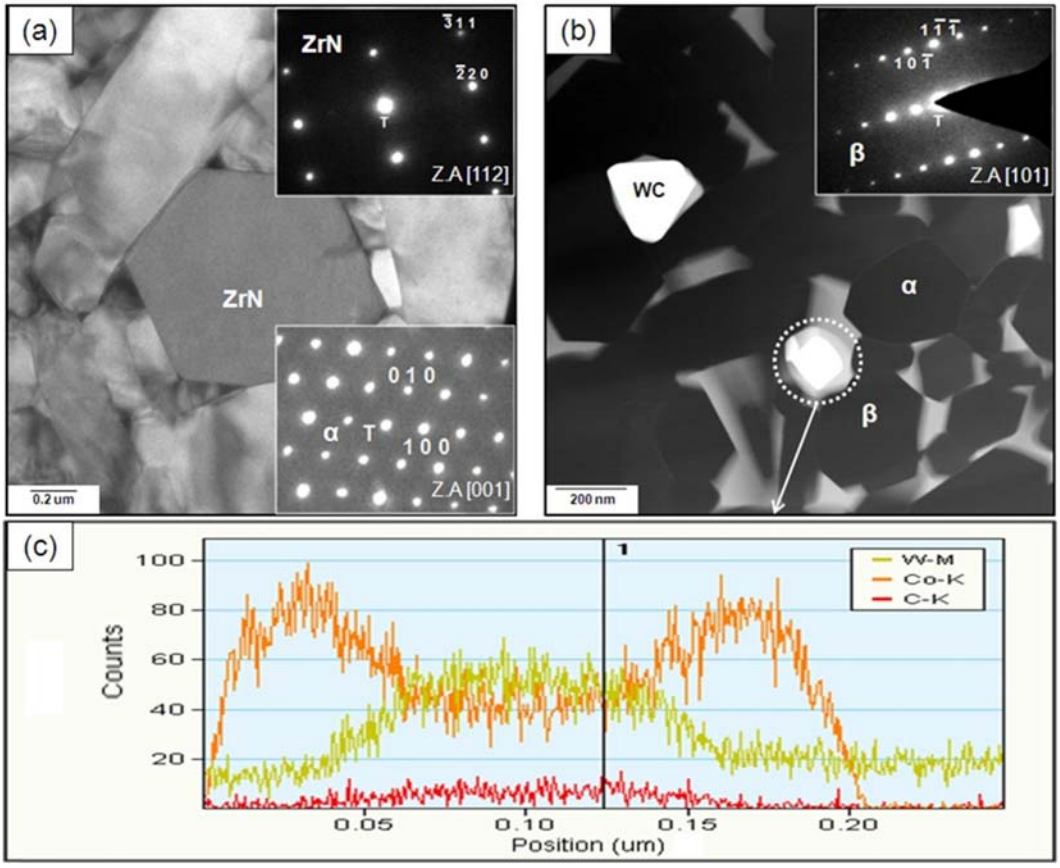

Fig. 5. TEM images of (a) SNZ sample, showing the α-SiAlON and ZrN phases and (b) SNW sample, showing the presence of β- SiAlON and WC, and (c) EDS line profile for SNW sample showing the core-shell structured WC-Co_3W_3C phase.

Table 2. Density and mechanical properties of the samples prepared using GPS and SPS [8]

Specimens	Gas Pressure Sintering (GPS)			E (GPa)	Spark Plasma Sintering (SPS)	
	Density (g/cm^3)	Hv (GPa@98N)	K_{IC} (MPa·m$^{1/2}$)		Hv (GPa@98N)	K_{IC} (MPa·m$^{1/2}$)
SNA	3.2618	18.13	4.62	316.84	18.7	4.09
SNZ	3.2916	17.72	4.75	317.23	18.0	4.36
SNW	3.3284	16.99	4.77	313.30	17.8	4.73

the nitridation of zirconia wear debris in SNZ, whereas WC and Co_3W_3C were formed from the cemented tungsten carbide wear debris in the SNW sample, as confirmed by XRD (Fig. 1). Regarding the effects of WC, Ayas *et al.* added WC intentionally to SiAlON and observed the formation of tungsten silicide (W_5Si_3) with WC-added SiAlON, which acted as a de-coloration pigment [11]. Although WC was formed in the SNW sample, however, no W_5Si_3 was found in this study and a previous study using SPS [8].

Figure 5(a) shows a TEM image of the SNZ sample, revealing the presence of α-SiAlON and ZrN phases, according to the corresponding selected area electron diffraction (SAED) patterns. The zone axes were [001] and [112] for α-SiAlON and ZrN, respectively. Figure 5(b) shows HAADF. TEM image of the SNW sample along with the SAED pattern with the [101] zone axis for β-SiAlON, were the black- and gray-colored regions correspond to the α- and β-SiAlON phases in the HAADF image, respectively. The analyzed crystal structure and space group information of each grain were matched with the XRD analysis results. The EDS line profiling results shown in Fig. 5(c) for the SNW sample suggested that the wear debris existed in the form of WC and formed a core-shell structured WC-Co_3W_3C phase in the grain boundaries. In Fig. 5(c), the pink and blue lines indicate W-Mα and W-Kα, respectively, whereas the red, lime green and green lines correspond to C-Kα, Co-Kα and Cu-Kα. According to the results, the amount of Co decreased from the outer layer to the inner area, whereas the existence of Co_3W_3C was confirmed by XRD, as shown in Fig. 2. These results show that the color and microstructure of the sintered SiAlON is affected by the milling media due to contamination.

As shown in Table 2, the density of the sintered SNA, SNZ and SNW samples was 3.26, 3.29, and 3.33 g/cm^3, respectively, indicating a higher SiAlON density in the order of alumina, zirconia and CTC milling media. The hardness was also affected by the milling media. The Vickers hardnesses for SNA, SNZ and SNW were 18.13, 17.27 and 16.99 GPa, respectively, which is proportional to the fraction of α-SiAlON in the sintered body. The density of the GPS-sintered samples was similar, whereas the hardness decreased slightly from the results obtained by SPS [8], due to the different amounts of α, β-SiAlON and grain boundary phases. The fracture toughness of the GPS-sintered samples was slightly higher than the SPS-sintered specimens, which could be explained using the increased SiAlON grain size, as shown in Fig. 3. The Young's modulus for SNA, SNZ and SNW were 316.84, 317.23 and 313.30 GPa, respectively, which are quite high values.

Table 3 lists high temperature Vickers hardness at room temperature, 300, 600 and 900 °C for 3 types of samples. SNA showed the highest hardness between room temperature to 600 °C, whereas SNZ showed the highest value at 900 °C. On the other hand, the SNZ sample showed the smallest decreasing rate in hardness by increasing the temperature, even though there was no significant difference among the specimens. The flexural strengths of the SNA, SNZ and SNW specimens based

Table 3. High temperature Vickers hardness results for 3 types of samples (GPa, load: 9.8N)

Specimens	Room Temp.	300 °C	600 °C	900 °C
SNA	19.49	14.71	13.72	12.04
SNZ	18.30	14.18	13.24	12.29
SNW	18.30	14.43	13.13	11.80

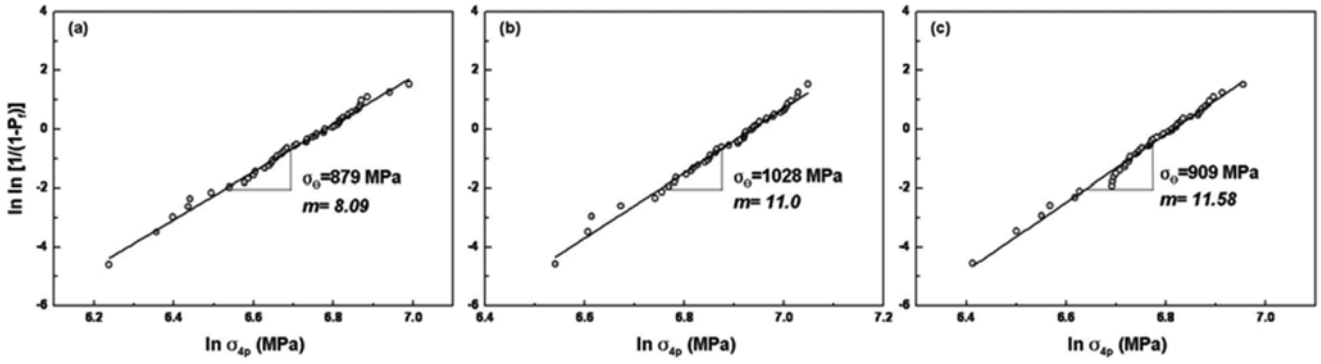

Fig. 6. Estimation of the Weibull modulus and Weibull characteristic strength of (a) SNA, (b) SNZ and (c) SNW samples.

on the 4-point bending test were 879, 1028 and 909 MPa, respectively, which are relatively high values considering the current commercialized SiAlON. The Weibull modulus data in Fig. 6 indicates the SNW sample to have highest value, even though the difference with the SNZ sample was not large. These overall variations with the mechanical properties can be attributed to the different amounts of SiAlON and secondary phases existing in the grain boundaries, which originated from the effect of the different milling media. Although all samples exhibited adequate physical and mechanical properties for the industrial applications of SiAlON, the SNZ sample milled with ZrO_2 media showed better properties than the SNA and SNW samples.

4. CONCLUSIONS

α/β-SiAlON composites were consolidated *in-situ* by a gas pressure sintering (GPS) at 1750 ℃ for 1.5 h. The results were compared with those obtained by spark plasma sintering (SPS). The type of milling media affected the formation of α-, β-SiAlON and grain boundary phases, which is very important for the physical and mechanical properties of sintered α/β-SiAlON composites, such as density, color, microstructure, hardness, fracture toughness, elastic modulus and flexural strength. The color of the specimens sintered by GPS was different due to the different inclusions and grain boundary phases, which originated from the milling media, similar to the results obtained by SPS. The room temperature hardness of the GPS-sintered specimens was lower than those by SPS, whereas the fracture toughness was higher. These were explained by the different grain sizes, α-SiAlON contents and grain boundary phases. Based on the results obtained, the SNZ sample prepared using ZrO_2 media showed excellent mechanical properties including hardness at high temperatures, making it the optimal condition for industrial use as a cutting tool.

ACKNOWLEDGEMENTS

This research was supported by the 2014 Yeungnam University Research Grant.

REFERENCES

1. P. Campbell, T. Laoui, J. P. Celis, and O. Van Der Biest. *Mat. Sci. Eng. A-struct.* **207**, 72 (1996).
2. M. I. Jones, K. Hirao, H. Hyuga, Y. Yamauchi, and S. Kanzaki, *J. Eur. Ceram. Soc.* **23**, 1743 (2003).
3. B. Bitterlich, S. Bitsch, and K. Friederich, *J. Eur. Ceram. Soc.* **28**, 989 (2008).
4. T. Ekström, P.-O. Käll, M. Nygren, and P.-O. Olsson, *Mat. Sci. Eng. A-struct. Mater.* **105-106**, 161 (1988).
5. P. L. Wang, H. Y. Tu, H. Wang, W. Y. Sun, and D. S. Yan, *Mater. Lett.* **28**, 373 (1996).
6. M. Herrmann and O. Goeb, *J. Eur. Ceram. Soc.* **21**, 303 (2001).
7. M. Herrmann and O. Goeb, *J. Eur. Ceram. Soc.* **21**, 461 (2001).
8. S. Chun, B.-K. Min, Y.-H. Han, Y.-M. Kim, K. Lee, Y. G. Jung, K.-H. Kim, Y.-K. Kim, and S. Kim, *Met. Mater. Int.* **19**, 163 (2013).
9. G. Grand, J. Demit, J. Ruste, and J. P. Torre, *J. Meter. Sci.* **14**, 1749 (1979).
10. B. R. Lawn and E. R. Fuller, *J. Mater. Sci.* **10**, 2016 (1975).
11. E. Ayas, A. Kara, H. Mandal, S. Turan, and F. Kara. *Mater. Lett.* **58**, 1498 (2004).
12. G.-J. Oh, K. Lee, D.-J. Lee, H.-P. Lim, K.-D., Yun, J.-S., Ban, K.-K. Lee, J. G. Fisher, and S.-W. Park, *Met. Mater. Int.* **18**, 805 (2012).